Received: 16 November 2019 | Revised: 12 January 2020 | Accepted: 19 March 2020

DOI: 10.1002/mmce.22236

RESEARCH ARTICLE

INTERNATIONAL JOURNAL OF RF AND MICROWAVE COMPUTER-AIDED ENGINEERING WILEY

Design and analysis of a quad-band substrate-integrated-waveguide cavity backed slot antenna for 5G applications

Tayfun Okan

Department of Electrical and Electronics Engineering, University of Turkish Aeronautical Association, Ankara, Turkey

Correspondence
Tayfun Okan, Bahcekapi Quarter Okul St. No: 11, University of Turkish Aeronautical Association, 06790, Ankara, Turkey.
Email: tokan@thk.edu.tr

Abstract

A planar and compact substrate integrated waveguide (SIW) cavity backed antenna and a 2 × 2 multi-input multi-output (MIMO) antenna are presented in this study. The proposed antenna is fed by a grounded coplanar waveguide (GCPW) to SIW type transition and planned to be used for millimeter-wave (mm-wave) fifth generation (5G) wireless communications that operates at 28, 38, 45, and 60 GHz frequency bands. Moreover, the measured impedance bandwidth ($|S_{11}| \leq -10$ dB) of the antenna covers 27.55 to 29.36, 37.41 to 38.5, 44.14 to 46.19, and 57.57 to 62.32 GHz bands and confirms the quad-band characteristic. Omni-directional radiation characteristics are observed in the far-field radiation pattern measurements of the antenna over the entire operating frequency. The reported antenna is compact in size ($9.7 \times 13.3 \times 0.6$ mm^3) and the gain values at each resonance frequency are measured as 3.26, 3.28, 3.34, and 4.51 dBi, respectively. Furthermore, the MIMO antenna performance is evaluated in terms of isolation, envelope correlation coefficient and diversity gain.

KEYWORDS

cavity backed antenna, fifth generation, grounded coplanar waveguide, quad-band, substrate integrated waveguide

1 | INTRODUCTION

With the increasing number of high-tech electronic devices, there is an increasing demand on high data rate and wide bandwidth to provide reasonable quality of service (QoS). Moreover, in the near future many electronic devices such as smart phones, laptops, security appliances, sensors, automobile applications, health care and wearable devices will all be in connection with each other with the introduction of internet of things (IoT). However, current systems and microwave frequency devices are not suitable to fulfill all these demands. Therefore, millimeter wave (mm-wave) fifth generation (5G) wireless communication technology, which is expected to launch worldwide in 2020/2021, is a promising technology with its wide bandwidth.

Some of the frequency bands recommended for 5G mobile communications are: 28, 38, 45, 60, and 70 GHz.[1] Among them the 28 GHz and 38 GHz bands are more advantageous, as there is a linear correlation between operating frequency and the design complexity of the antenna. Besides that, with the increasing frequency signal propagation loss and atmospheric attenuation also increases.[2] Moreover, multiband capability is an important attribute for 5G antennas that avoids using a separate antenna or device for different operating frequencies. Hence, employing a single antenna operable at different frequency bands degrades the costs and required free space in the device.

With the increasing interest in mm-wave, substrate integrated waveguide (SIW) technique has been frequently used in many antennas,[3-10] where plated through hole vias connect the top and ground planes. Sidewalls are created and more importantly rectangular waveguide is built into a printed circuit board (PCB) with the alignment of the

vias. Moreover, compared to conventional transmission lines SIW has less interference, less radiation loss and excellent isolation.[5] Besides these advantages one major drawback of SIW is that the fabrication quality of the antenna is very crucial. If the gap between the sidewalls varies side to side, that may cause problems and leakage as the wavelength is very small with mm-wave operating frequencies. SIW antenna structures have been used with microstrip to SIW transition and grounded coplanar waveguide (GCPW) to SIW transition. However, especially for mm-wave frequency applications, GCPW to SIW transition performs better than the former one.[9]

Single band and dual band mm-wave antennas for 5G applications were studied in References.[1 and 10-19] In some of them via-free microstrip-fed patch antennas were used, while in others SIW antennas were analyzed. As the number of operable bands of the antenna increased, the bandwidth at these operating frequencies generally seemed to decrease. In Mahmoud and Montaser,[20] the design and analysis of a tri-band mm-wave antenna was performed for using in 5G mobile base stations. Another tri-band (28/38/61 GHz) mm-wave antenna was reported in Reference 21. However, the proposed antenna was unable to cover the 60 GHz frequency and it had a very narrow bandwidth especially at 61 GHz band.

To the best of author's knowledge, currently there is not any study on literature in which an antenna is designed that is operable in four different 5G wireless communication bands. In this study, a SIW cavity backed rectangular slot antenna and its 2×2 multi-input multi-output (MIMO) version are presented, where GCPW is employed to excite the three longitudinal rectangular slots with different dimensions. The reason to etch multiple slots with different lengths and widths is to make the antenna radiate at the desired resonance frequencies and to create a quad-band radiation characteristic. Thanks to its simplicity, our proposed design has several benefits including more practical fabrication process and better mechanical performance, when compared with presented methods in References 17 and 19. Moreover, the proposed antenna operates at four different 5G communication bands that are 28, 38, 45, and 60 GHz, respectively. It is also compact with a size of $9.7 \times 13.3 \times 0.6$ mm^3 ($0.89\lambda \times 1.22\lambda \times 0.055\lambda$, where λ is the wavelength at the lowest operating frequency). To validate the simulation results obtained by CST Microwave Studio, the antennas are fabricated and measured.

2 | ANTENNA DESIGN

The proposed quad-band SIW cavity backed antenna is depicted in Figure 1. The top and bottom copper layers are represented with yellow color and their thickness (T_c) is 0.035 mm. The vias that create the SIW cavity are indicated with blue and these vias connect the top and bottom copper plates to each other. The antenna is designed on a Rogers RO4003C substrate with a permittivity of 3.55, a loss tangent of 0.0027, and a thickness (T) of 0.6 mm. Table 1 list the optimized antenna parameters to achieve a wide impedance bandwidth.

As can be seen from Figure 1, the designed antenna normally has a smaller width, which is 8 mm (W_9). But in order to connect the antenna and PCB edge launch connector sturdily, two U-shaped slots need to be formed on the substrate, on both left and right sides of the PCB. This causes an expansion on the width and makes it 13.3 mm (W). This expanded antenna ($9.7 \times 13.3 \times 0.6$ mm^3) has the same characteristic with the initially designed one ($9.7 \times 8 \times 0.6$ mm^3); therefore, the analysis is made by using the expanded antenna. The design and EM simulations presented in the following sections are performed with the help of CST Microwave Studio.

The function of the low profile SIW cavity is to improve the radiation performance. The metalized via arrays significantly improves gain and directivity; whereas prevents the undesired leakage and suppresses the effects of edge diffraction by reducing surface wave propagation over the substrate. Beside several benefits of SIW, there are also some major challenges especially when used with mm-wave applications. Depending on the design, there may occur some radiation loss through the gap between the plated through hole vias. Thus, in order to prevent leakage through the gaps, $D \le \lambda_g/5$ and $S \le 2D$ conditions should be considered when designing the antenna.[8] The D and S parameters represents diameter of the via and spacing between the vias, respectively; where λ_g is the wavelength for the highest operating frequency.

The relationship between the resonance frequency of the planar cavity resonator and geometrical parameters related to antenna dimensions can be derived by using the following equations.[3]

$$f_{mnp} = \frac{1}{2\sqrt{\mu_r \varepsilon_r}} \sqrt{\left(\frac{m}{L_{\text{eff}}}\right)^2 + \left(\frac{n}{W_{\text{eff}}}\right)^2 + \left(\frac{p}{T}\right)^2} \quad (1)$$

$$W_{\text{eff}}\,(or\, L_{\text{eff}}) = W_{\text{SIW}}(\text{or}\, L_{\text{SIW}}) - 1.08\frac{D^2}{S^2} + 0.1\frac{D^2}{W_{\text{SIW}}\,(\text{or}\, L_{\text{SIW}})} \quad (2)$$

where m, n, p are TE or TM mode integers and T represents the thickness of the substrate. μ_r, ε_r, L_{eff}, and W_{eff} refer to permeability, permittivity, effective length and width of SIW cavity, respectively.

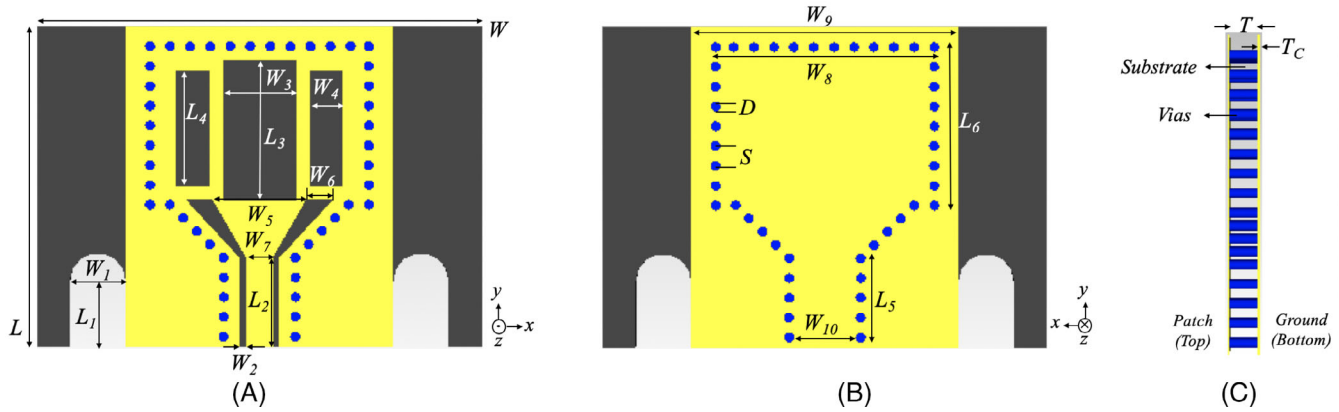

FIGURE 1 Geometrical configuration of the proposed antenna design (A) top view, (B) bottom view, and (C) side view

TABLE 1 Dimensions of the antenna element

Parameter	W	L	D	S	W_1	W_2	W_3	W_4	W_5	W_6
value (mm)	13.3	9.7	0.3	0.6	1.66	0.2	2.2	1	2.8	0.8
Parameter	W_7	W_8	W_9	W_{10}	L_1	L_2	L_3	L_4	L_5	L_6
value (mm)	0.8	6.85	8	1.85	2	2.7	4.23	3.5	2.7	5.1

In order to obtain the resonance frequencies at the desired values, slots are introduced inside the SIW cavity. As a result of the design studies it is observed that if the slot length is larger than its width, then resonance frequencies occur at lower frequencies. If the width is larger than the length, then resonance frequencies occur at higher values of the frequency range. Therefore, three rectangular shaped slots, the widths of which are smaller than their lengths ($W_3 < L_3$, $W_4 < L_4$), are used to obtain the required resonance at low frequencies. These slots are aligned in parallel to improve the impedance bandwidth by enlarging the total slot width and also to create the desired resonance at higher frequencies as well.

Seven step procedure is followed in the antenna design process, which is given in detail step by step below. This procedure can be followed when desinging any type of antenna.

1 Determine the aim and reason to design the antenna.
2 Choose proper substrate material with respect to its permittivity and conductivity value.
3 Decide the feeding technique that needs to be used: microstrip, coaxial, GCPW, etc.
4 Determine approximate length and width values for desired resonance frequencies, and also substrate thickness by using valid equations.
5 Simulate the designed antenna by using computer based EM tool and observe the output values.
6 Optimize the parameters at the same time modifying the design of the antenna, until desired output values are reached.
7 Fabricate the antenna and perform the experimental measurements by using VNA and with the help of anechoic chamber. Compare and validate experimental results with simulation results.

The three successive design stages of the proposed antenna are displayed in Figure 2. The improvement and effect of each design stage on resonance frequency and impedance bandwidth is shown in Figure 3, where frequency vs reflection coefficient (S_{11}) relationship is plotted. In Antenna-1, SIW cavity structure is generated by positioning the vias with the help of the aforementioned equations and conditions. This antenna does not radiate properly as it does not have any radiative aperture; which is also observed from the reflection coefficient curve of Antenna-1 in Figure 3.

In the first evolution step, GCPW transmission is introduced to form the GCPW to SIW feeding transition. With this stage, the impedance bandwidth is enhanced ($|S_{11}| \leq -10$ dB) and resonance frequencies are created at 28.3, 36.3, 45.4, 53.7, and 59.2 GHz frequencies as seen in Figure 3. One important factor for the further design stages is that, the slots carved on the surface of the SIW cavity should be resonance at the desired operating frequencies, in order to achieve the highest radiation efficiency. Hence, the position and dimension of the slot also plays an important role in this process. Antenna-3 is derived by etching two parallel rectangular shaped slots inside the SIW cavity. This results an improvement in the impedance bandwidth at 36.3 and 45.4 GHz frequency bands. However, two desired resonance frequencies for 5G applications at 38 and 60 GHz

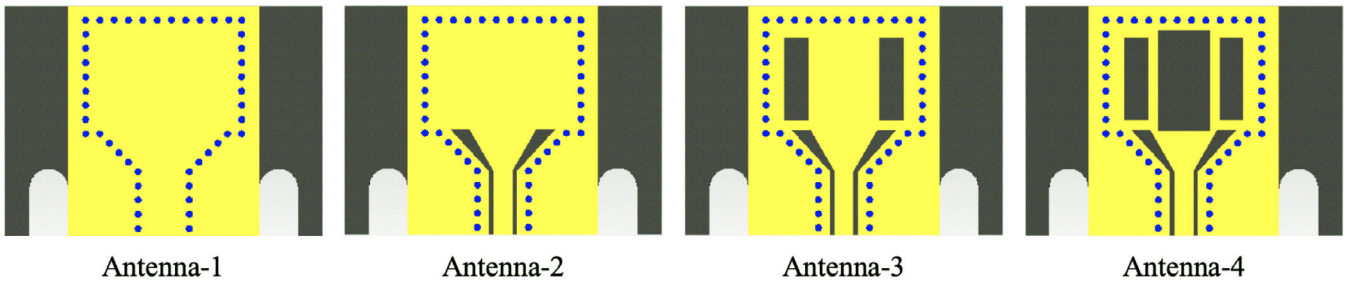

FIGURE 2 Design stages of the proposed antenna

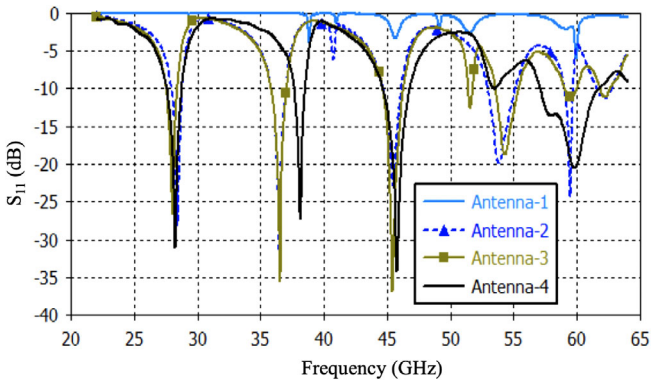

FIGURE 3 Simulated reflection coefficient curves for each design stage

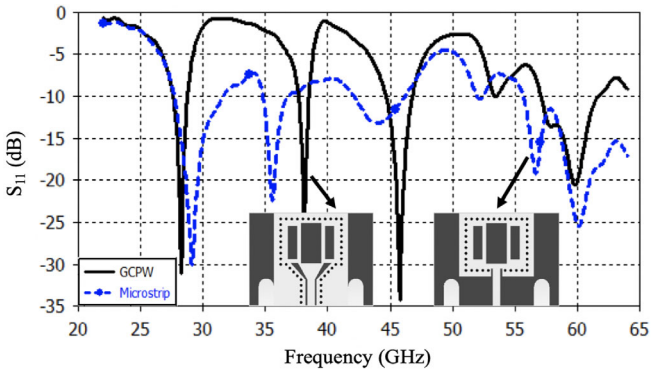

FIGURE 4 Reflection coefficient graph for GCPW and microstrip fed antennas

where $|S_{11}| \leq -10$ dB are still missing. Therefore, in the last design stage a third rectangular slot is positioned in the middle of the cavity and the proposed antenna is created. This third slot is placed parallel to the other two slots to create a resonance frequency at a higher frequency value (60 GHz) by increasing the total width of the slots. With the final design stage, four resonance frequencies are achieved at 28.26, 38.13, 45.77, and 59.82 GHz, as seen in Figure 3.

To analyze the effect of feeding type on radiation characteristic, the slotted radiating elements are fed by both GCPW to SIW and microstrip to SIW transitions. As seen from the reflection coefficient graph in Figure 4, the simulated antennas do not have completely different characteristics. Both have four operating frequency bands and have similar resonance frequencies. But, the GCPW fed antenna has better impedance matching and resonates perfectly at the desired frequencies. Hence, the GCPW fed antenna performs better than the former one.

With respect to conventional antenna theory, the impedance bandwidth of the antenna is proportional to the thickness of the substrate or width of the slots. For that reason, a parametric study is performed and the effect of some parameters on antenna performance is investigated. First, the effect of the width of the middle rectangular slot on reflection coefficient is analyzed. As seen in Figure 5A, the optimum performance is obtained with 2.2 mm value. With 1.9 mm, the impedance bandwidth is decreased at 45 and 60 GHz bands. Moreover, an undesirable band is created at 53.12 GHz where $|S_{11}| \leq -10$ dB. Similarly, a reduction in bandwidth is observed at 60 GHz band with 2.5 mm value.

Another parameter that effects the performance of the antenna is substrate thickness. As seen in Figure 5B, an undesirable band is created at 53.7 GHz for 0.5 mm value and a smaller bandwidth at 60 GHz band is obtained with 0.7 mm. Thus, optimum performance characteristic is reached with 0.6 mm value.

3 | RESULTS AND DISCUSSION

The proposed antenna is fabricated and experimental measurements are obtained with the help of Anritsu 37397A Vector Network Analyzer (VNA). The maximum operating frequency in this study is approximately 63 GHz. Therefore, a 1.85 mm edge launch PCB connector, which provides a maximum operating frequency of 67 GHz, is employed to excite the antenna in the experimental measurements.

Four resonance frequencies are observed in the SIW cavity which are at 28.47, 38.04, 44.95, and 60.47 GHz, as seen in Figure 6. The 10 dB impedance bandwidths at

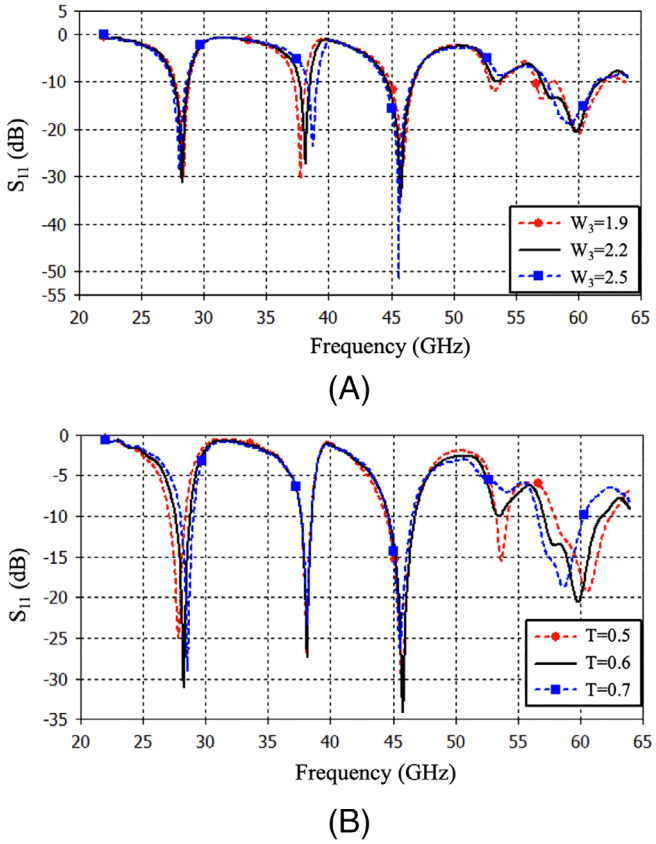

FIGURE 5 The effect of (A) W_3 and (B) T on reflection coefficient

each of these resonance frequencies are measured as 1.81 GHz (27.55-29.36 GHz), 1.09 GHz (37.41-38.5 GHz), 2.05 GHz (44.14-46.19 GHz), and 4.75 GHz (57.57-62.32 GHz), respectively. Similarly, the fractional bandwidth percentage values are obtained as 6.36%, 2.87%, 4.54%, and 7.92%, respectively. A good agreement is achieved between the simulated and measured reflection coefficient curves, as seen in Figure 6. Table 2 points out the simulated and measured bandwidths for each operating band. The fabricated antenna and the measurement setup in the anechoic chamber are depicted in Figure 7.

As seen in Figure 8A, the measured realized gain at each resonance frequency is 3.26, 3.28, 3.34, and 4.51 dBi, respectively. Moreover, the measured radiation efficiency of the proposed antenna is shown in Figure 8B, which is obtained at each resonance frequency as 57.6%, 58.4%, 55.7%, and 82%, respectively. As seen from Figure 8A, B, the realized gain and radiation efficiency values increase with the increasing frequency. This behavior is predictable and it can be justified in some ways.[22] The main reason of the degredation in the realized gain and radiation efficiency at lower operating frequencies is that, the antenna exhibits omni-directional radiation characteristics at lower

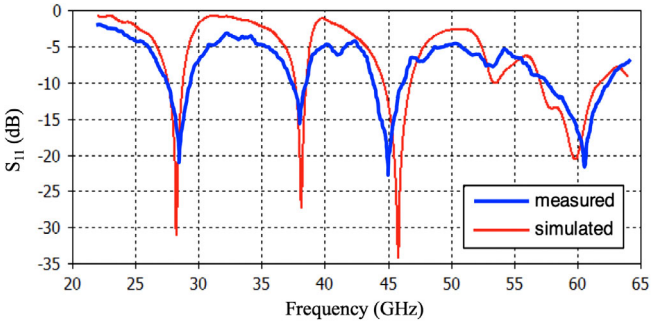

FIGURE 6 The measured and simulated reflection coefficient graph

frequencies; on the other hand, it tends to exhibit slightly directional properties at higher frequencies. Moreover, all these results are suitable for short range wireless communicaiton applications.

The two dimensional vectoral current distribution for each resonance frequency of the proposed antenna is shown in Figure 9. With respect to the designed geometry, two thin copper lines exist between each of three rectangular slots. The surface currents are forced to pass through these lines, therefore a concentration occurs and current density increases at these regions. As seen from Figure 9A, B, the black arrows indicate the direction of the surface currents on the antenna. The second region, where the surface current density of the antenna is mainly concentrated is along the GCPW transition slots. As the frequency increases, the current density around the side edges of the three rectangular slots decreases; whereas, it increases around the GCPW transition region.

The measured and simulated far-field radiation patterns of the proposed antenna are shown for each resonance frequency in Figure 10. The top quartet show the *E*-plane (*xz*-plane) results and the bottom quartet depict the *H*-plane (*yz*-plane) measurements. As seen from the graphs, the co-polarized fields in *H*-plane and cross-polarized fields in *E*-plane retain their omni-directional properties at any frequency; whereas, the co-polarized fields in *E*-plane have unidirectional radiation patterns. The level of cross-polarized fields in *H*-plane are below −93 dB, which makes them too small to appear in the graph at each frequency. As the frequency increases, the sidelobes tends to appear for cross-polarized fields in *E*-plane. However, the proposed antenna maintains its radiation characteristics throughout the operating bandwidth with little deviations.

Table 3 compares some of the properties of the proposed antenna with other mm-wave antennas designed for 5G applications. As seen from the table, the proposed antenna is the only one that operates at four different

TABLE 2 Simulated and measured bandwidth (fractional bandwidth) at 28, 38, 45, and 60 GHz bands

	Operating band (GHz)			
	28	**38**	**45**	**60**
Simulated	27.58-28.76 (4.19%)	37.62-38.5 (2.31%)	44.64-46.78 (4.68%)	57.07-61.75 (7.85%)
Measured	27.55-29.36 (6.36%)	37.41-38.5 (2.87%)	44.14-46.19 (4.54%)	57.57-62.32 (7.92%)

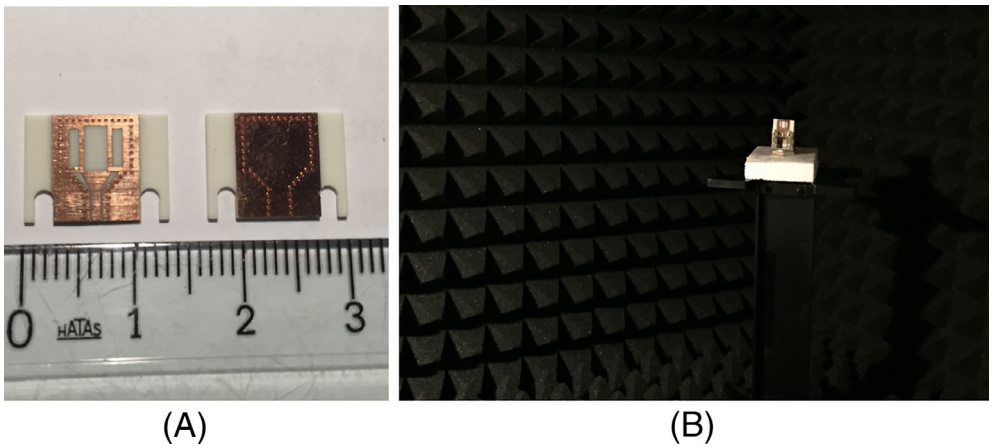

FIGURE 7 The proposed antenna (A) as a fabricated prototype and (B) in an anechoic chamber

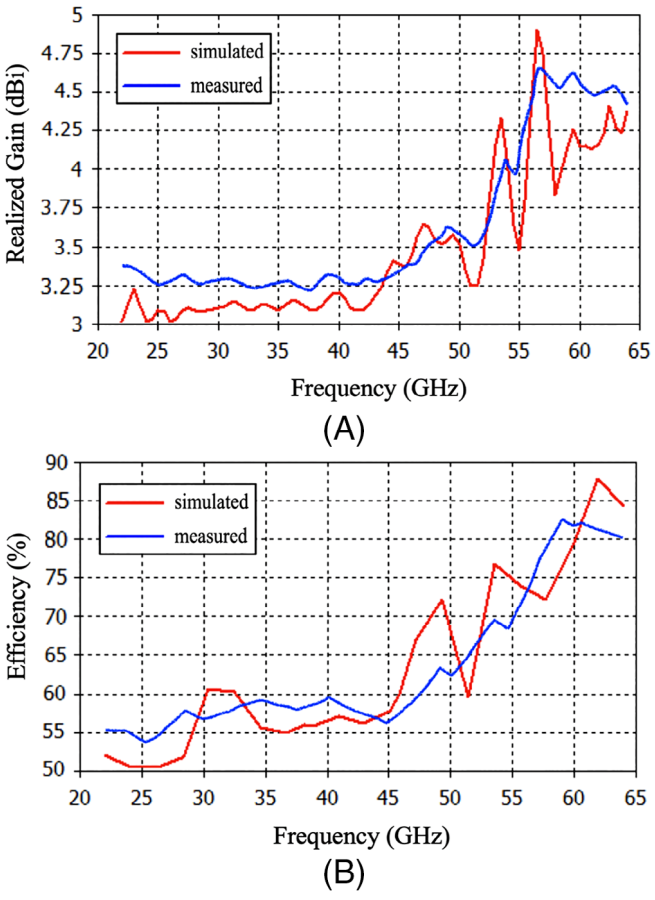

FIGURE 8 Measured and simulated (A) realized gain and (B) radiation efficiency of the proposed antenna

frequency bands. When the bandwidths are compared, the impedance bandwidths of the presented antenna are slightly narrower than others. Additionally, most of the studies include array antennas, thus the proposed antenna is the smallest in size apart from the ones reported in References 1 and 16.

4 | 2 × 2 MIMO ANTENNA

Under this title, a 2 × 2 MIMO antenna is presented based on the proposed antenna in the previous section. The proposed antenna is linearly polarized; therefore, positioning the two antenna elements orthogonal to each other to construct the MIMO structure provides polarization diversity. This is a frequently used method for dual polarized MIMO antenna structures.[19,20] The orthogonally placed antenna elements are shown in Figure 11A, where the finalized MIMO antenna width and length are 17.7 and 9.7 mm, respectively. The proposed MIMO antenna is again printed on Rogers RO4003C substrate material with a dielectric constant of 3.55, a loss tangent of 0.0027, and a thickness of 0.6 mm. As aforementioned, the substrate of the antenna is extended on both sides of the radiator to form a U-shaped slot and properly connect the PCB edge launch connector. This $(W - W_9)/2$ length extension provides two benefits: (a) the left radiating element of the MIMO structure is shifted slightly upwards; thus, it is not affected by the edge launch connector of

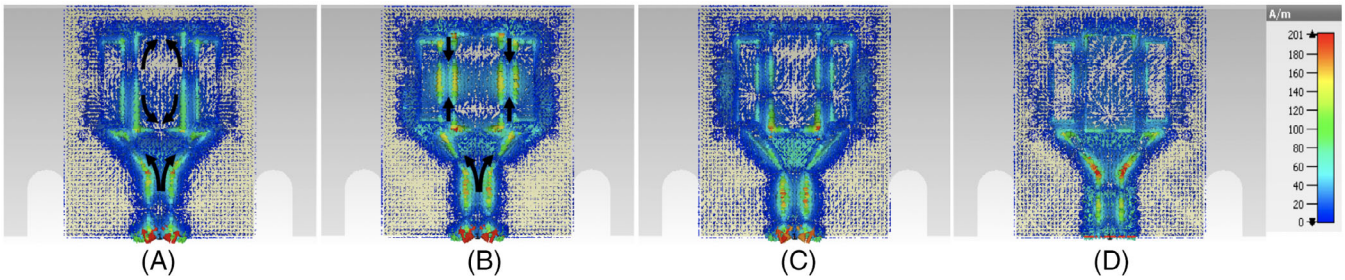

FIGURE 9 Vectoral surface current distribution at (A) 28.26 GHz, (B) 38.13 GHz, (C) 45.77 GHz, and (D) 59.82 GHz

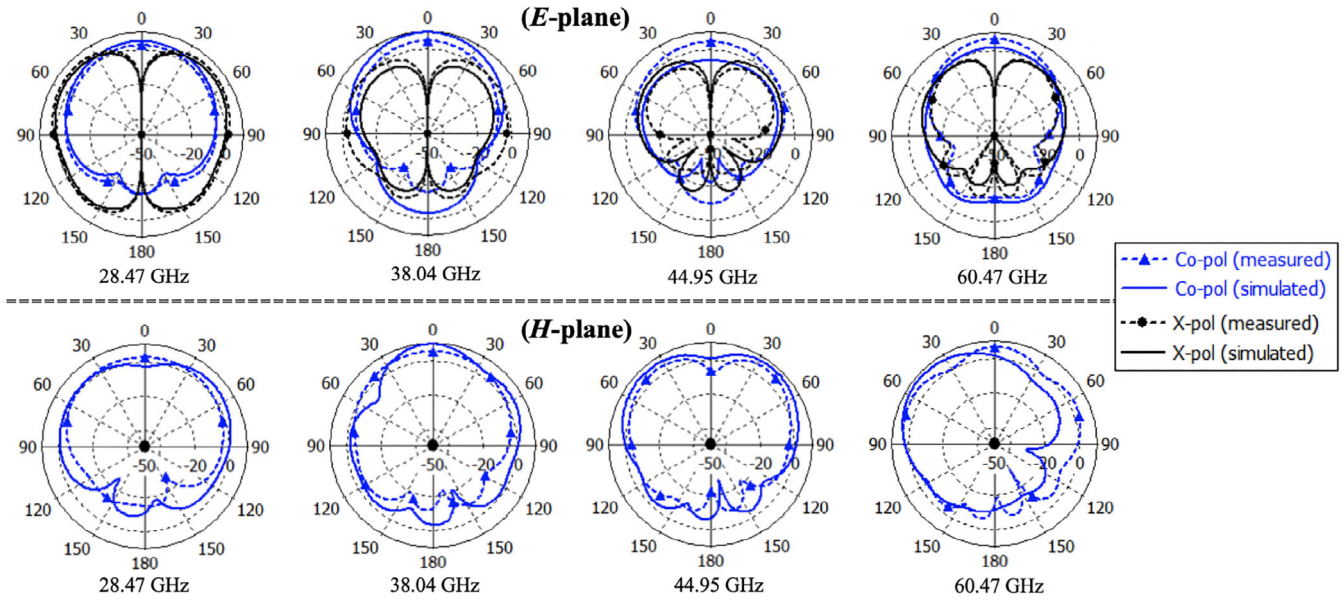

FIGURE 10 Antenna far-field radiation patterns for *E*-plane and *H*-plane at 28.47, 38.04, 44.95, and 60.47 GHz

TABLE 3 Comparison with other state-of-arts in literature

References	Spectrum (GHz)	Bandwidth (GHz)	Area (mm^2)	Via design	Substrate permittivity
[11]	28	26.9-29	30×19.9 ($2.69\lambda \times 1.78\lambda$)	No	2.2
[14]	38	36.3-40.9	30×15 ($3.63\lambda \times 1.82\lambda$)	No	3.0
[15]	45	43.08-47.8	12.7×15.8 ($1.82\lambda \times 2.26\lambda$)	Yes	2.2
[16]	28/38	27.57-28.42 37.62-38.37	6.8×6.8 ($0.63\lambda \times 0.63\lambda$)	No	2.2
[1]	28/45	27.4-28.6 44.7-45.7	6×6 ($0.55\lambda \times 0.55\lambda$)	No	2.2
[17]	60/70	57–71	14.4×14.4 ($2.74\lambda \times 2.74\lambda$)	Yes	2.2
[18]	28/38	26.65-29.2 36.95-39.05	14×12 ($1.24\lambda \times 1.07\lambda$)	No	2.2
[19]	38/48	37.09-37.91 47.13-48.47	15.4×8 ($1.9\lambda \times 0.99\lambda$)	Yes	2.2
[20]	28/38/48	25.5-29.5 35.5-39.9 45-49	34.8×34.8 ($2.96\lambda \times 2.96\lambda$)	No	2.2
Proposed	28/38/45/60	27.55–29.36 37.41-38.5 44.14-46.19 57.57-62.32	9.7×13.3 ($0.89\lambda \times 1.22\lambda$)	Yes	3.38

Abbreviation: λ, wavelength at the lowest operating frequency.

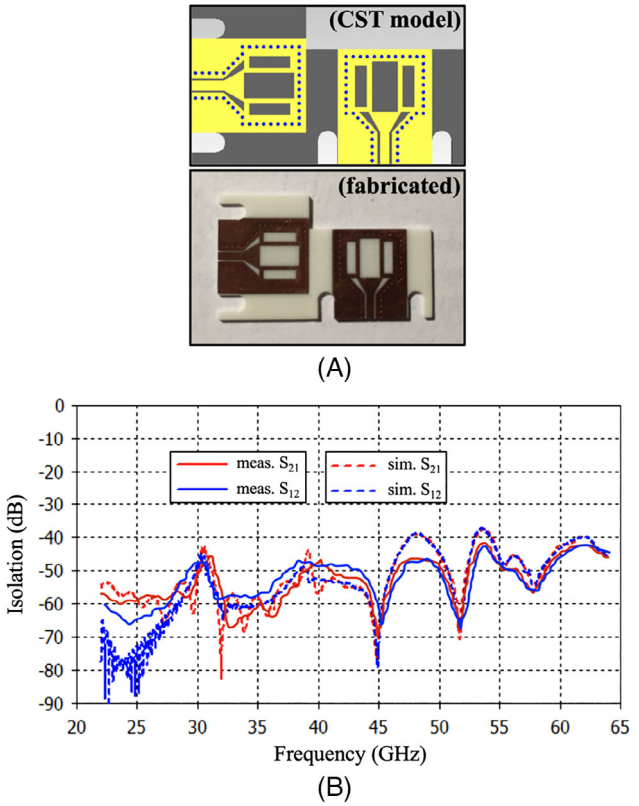

FIGURE 11 (A) The proposed 2 × 2 MIMO antenna and its (B) isolation result

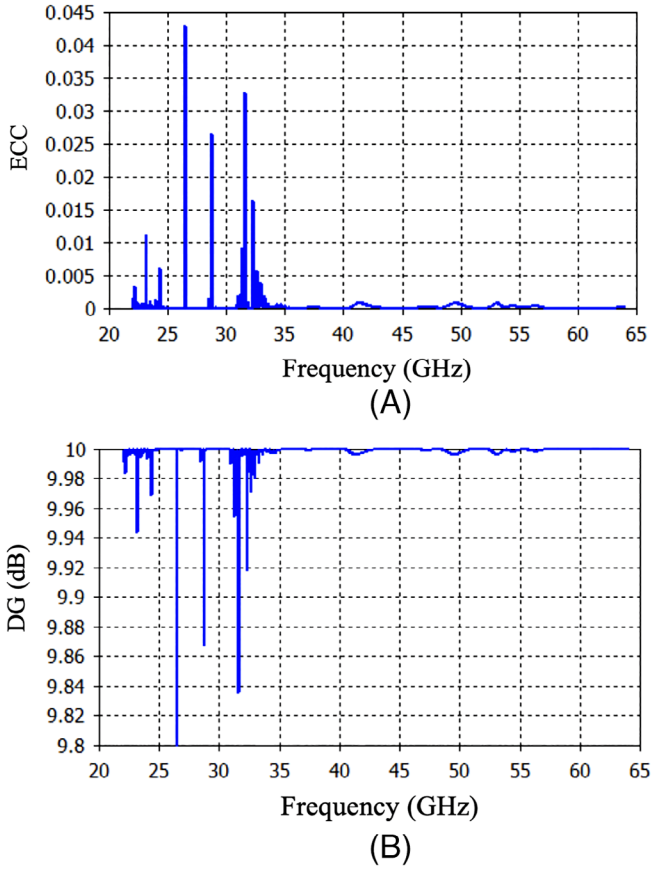

FIGURE 12 The 2 × 2 MIMO antenna results of (A) envelope correlation coefficient and (B) diversity gain

the right element, and (b) there occurs a distance between the orthogonally placed radiator elements and this prevents the mutual coupling between the radiating elements.

The characteristic of the reported 2 × 2 MIMO antenna is examined by using several performance metrics. Figure 11B represents the simulated and measured insertion loss (S_{12} and S_{21}), in other words the isolation, of the proposed MIMO antenna. As seen from the figure, the isolation is nearly below 40 dB within the operating frequency. Envelope correlation coefficient (ECC) and diversity gain (DG) are another performance metrics used for the performance analysis of MIMO antennas. The mathematical definition of ECC is made by using reflection coefficient and insertion loss parameters as seen in Equation (3). Moreover, DG is mathematically related to ECC by Equation (4). As seen from Figure 12, the simulated ECC is <0.005 in the operating frequency bands, this demonstrates that the mutual coupling between the antenna elements is very low. Furthermore, the simulated DG value reaches the highest value of 10 dB and lowest value of 9.98 dB, which are desirable values for a MIMO antenna.

$$\mathrm{ECC} = \frac{\left|S_{11}^{*}S_{12} + S_{21}^{*}S_{22}\right|^{2}}{\left(1-\left(|S_{11}|^{2}+|S_{21}|^{2}\right)\right)\left(1-\left(|S_{22}|^{2}+|S_{12}|^{2}\right)\right)} \quad (3)$$

$$DG = 10\sqrt{1-\mathrm{ECC}} \quad (4)$$

5 | CONCLUSION

A cavity backed slot antenna based on SIW technique and its 2 × 2 MIMO version are tested and analyzed. The proposed antenna is fed by GCPW type transition and fabricated meticulously on two layer PCB. Three rectangular shaped slots are introduced to resonate the antenna at 28, 38, 45, and 60 GHz frequencies. Furthermore, several performance characteristics of the antenna are analyzed with the help of simulation results and experimental measurements. Owing to its ease of fabrication, low profile, light weight, and compatibility to operate at four different frequency bands; the proposed antenna is expected to be a preferable candidate to be used with smart phones, tablets or any other portable device that operates various 5G applications.

ORCID

Tayfun Okan https://orcid.org/0000-0002-9913-0803

REFERENCES

1. Khattak MI, Sohail A, Khan U, et al. Elliptical slot circular patch antenna array with dual band behaviour for future 5G mobile communication networks. *Prog Electromagn Res C*. 2019;89:133-147.
2. Kuzu S, Akcam N. Array antenna using defected ground structure shaped with fractal form generated by Apollonius circle. *IEEE Antennas Wirel Propag Lett*. 2017;16:1020-1023.
3. Luo GQ, Hu ZF, Liang Y, et al. Development of low profile cavity backed crossed slot antennas for planar integration. *IEEE Trans Antennas Propag*. 2009;57(10):2972-2979.
4. Kumar A, Saravanakumar M, Raghavan S. Dual-frequency SIW-based cavity-backed antena. *AEU-Int J Electron C*. 2018;97:195-201.
5. Mukherjee S, Biswas A, Srivastava KV. Broadband substrate integrated waveguide cavity backed bow-tie slot antenna. *IEEE Antennas Wirel Propag Lett*. 2014;13:1152-1155.
6. Hua C, Liu M, Lu Y. Planar integrated substrate integrated waveguide circularly polarized filtering antenna. *Int J RF Microw Comput Aided Eng*. 2018;e21517. https://doi.org/10.1002/mmce.21517.
7. Priya S, Kumar K, Dwari S. Substrate integrated waveguide dual-frequency dual-sense circularly polarized cavity-backed slot antenna. *Int J RF Microw Comput Aided Eng*. 2019;e21987. https://doi.org/10.1002/mmce.21987.
8. Mungaru NK, Thangavelu S. Broadband substrate integrated waveguide venus-shaped slot antenna for V-band applications. *Microw Opt Technol Lett*. 2019;61(10):2342-2347.
9. Gharbi ME, Aknin N, Ahyoud S. Design of SIW cavity backed triangular slot antenna using two different feeding transitions. *Procedia Manuf*. 2019;32:687-693.
10. Chu QX, Li XR, Ye M. High-gain printed log-periodic dipole array antenna with parasitic cell for 5G communication. *IEEE Trans Antennas Propag*. 2017;65(12):6338-6344.
11. Park JS, Ko JB, Kwon HK, et al. A tilted combined beam antenna for 5G communications using a 28-GHz band. *IEEE Antennas Wirel Propag Lett*. 2016;15:1685-1688.
12. Mantash M, Kesavan A, Denidni TA. Beam-tilting endfire antenna using a single-layer FSS for 5G communication networks. *IEEE Antennas Wirel Propag Lett*. 2018;17(1):29-33.
13. Kornprobst J, Wang K, Hamberger G, et al. A mm-wave patch antenna with broad bandwidth and a wide angular range. *IEEE Trans Antennas Propag*. 2017;65(8):4293-4298.
14. Li S, Chi T, Wang Y, et al. A millimeter-wave dual-feed square loop antenna for 5G communications. *IEEE Trans Antennas Propag*. 2017;65(12):6317-6328.
15. Xie H, Belostotski L, Okoniewski M. A Q-band high-gain substrate-integrated waveguide slot antenna. *Microw Opt Technol Lett*. 2015;57(6):1370-1374.
16. Aliakbari H, Abdipour A, Mirzavand R, et al. A single feed dual-band circularly polarized millimeter-wave antenna for 5G communication. Paper presented at: Proceedings of European Conference on Antennas and Propagation (EuCAP); April 2016; Davos, Switzerland
17. Zhu Q, Ng KB, Chan CH, et al. Substrate-integrated-waveguide-fed array antenna covering 57-71 GHz band for 5G applications. *IEEE Trans Antennas Propag*. 2017;65(12):6298-6306.
18. Hasan MN, Bashir S, Chu S. Dual band omnidirectional millimeterwave antenna for 5G communications. *J Electromagnet Wave Appl*. 2019;33(12):1581-1590.
19. Wu Q, Yin J, Yu C, et al. Low-profile millimeter-wave SIW cavity-backed dual-band circularly polarized antenna. *IEEE Trans Antennas Propag*. 2017;65(12):7310-7315.
20. Mahmoud KR, Montaser AM. Performance of tri-band multi-polarized array antenna for 5G mobile base station adopting polarization and directivity control. *IEEE Access*. 2018;6:8682-8694.
21. Rehman MU, Adekanye M, Chattha HT. Tri-band millimetre-wave antenna for body-centric networks. *Nano Commun Netw*. 2018;18:72-81.
22. Amendola G, Arnieri E, Boccia L. Analysis of lossy SIW structures based on the parallel plates waveguide Green's function. *Prog Electromagn Res C*. 2012;33:157-169.

AUTHOR BIOGRAPHY

Tayfun Okan received the B.Sc. degree from Electrical and Electronics Engineering, Baskent University, Ankara, Turkey. He then received the M.S. and Ph.D. degrees from Electrical and Electronics Engineering Department of Gazi University in 2012 and 2018, respectively. He is currently working as an assistant professor in Electrical and Electronics Engineering Department, University of Turkish Aeronautical Association, Ankara, Turkey. His research interests are electrically small antennas, microwave/mm wave components and subsystems, high frequency techniques and radiation pattern analysis.

How to cite this article: Okan T. Design and analysis of a quad-band substrate-integrated-waveguide cavity backed slot antenna for 5G applications. *Int J RF Microw Comput Aided Eng*. 2020;30:e22236. https://doi.org/10.1002/mmce.22236